

Article

A Method for Predicting the Load Interaction between Reinforced Thermoplastic Pipe and Sandy Soil Based on Model Testing

Chuan Wang ^{1,2,3,*}, Lianghai Liu ^{1,2,3}, Ya Zhang ^{1,2,3} and Min Lou ^{1,2,3}

¹ College of Mechanical and Electronic Engineering, China University of Petroleum (East China), Qingdao 266580, China

² Key Laboratory of Unconventional Oil & Gas Development, China University of Petroleum (East China), Ministry of Education, Qingdao 266580, China

³ National Engineering Laboratory of Offshore Geophysical and Exploration Equipment, China University of Petroleum (East China), Qingdao 266580, China

* Correspondence: wangchuan@upc.edu.cn

Abstract: This study aims to investigate the interaction between reinforced thermoplastic pipes (RTPs) and sandy soil. The mechanical properties of sandy soil in the South China Sea region were determined through shear tests to obtain fundamental data. Subsequently, a specialized experimental setup was designed and assembled to study the pipe–soil interaction, specifically measuring the lateral soil resistance of flexible pipes at varying burial depths. Data analysis revealed the relationship between soil resistance, lateral displacement, and initial burial depth. To simulate the mechanical behavior of the pipe–soil interaction, the coupled Eulerian–Lagrangian (CEL) method was employed for numerical simulations. The research findings indicate that the lateral soil resistance is influenced by the uplift height and accumulation width of the soil ahead of the pipe. Within a lateral displacement range of 0.5 times the pipe diameter (0.5D), the lateral soil resistance rapidly increases, resulting in a soil uplift along the circumferential direction of the pipe. This process not only enhances the load-bearing capacity of the pipe but also increases the accumulated soil resistance, consequently expanding the soil failure zone. Furthermore, the ultimate soil resistance exhibits an increasing trend with an increasing burial depth. Once the pipe reaches a certain burial depth, the uplift height of the soil reaches a critical state. To address the grid distortion caused by soil deformation, numerical simulations based on the CEL method effectively modeled the pipe–soil interaction forces under significant lateral displacements, exhibiting good agreement with the experimental results. This study provides a solution for investigating soil resistance in submarine pipelines, thereby contributing significantly to the design and performance prediction of underwater pipelines.

Keywords: lateral soil resistance; CEL method; reinforced thermoplastic pipes (RTPs); pipe–soil interaction



Citation: Wang, C.; Liu, L.; Zhang, Y.; Lou, M. A Method for Predicting the Load Interaction between Reinforced Thermoplastic Pipe and Sandy Soil Based on Model Testing. *J. Mar. Sci. Eng.* **2023**, *11*, 2353. <https://doi.org/10.3390/jmse11122353>

Academic Editor: Dejan Brkić

Received: 4 November 2023

Revised: 11 December 2023

Accepted: 11 December 2023

Published: 13 December 2023



Copyright: © 2023 by the authors. Licensee MDPI, Basel, Switzerland. This article is an open access article distributed under the terms and conditions of the Creative Commons Attribution (CC BY) license (<https://creativecommons.org/licenses/by/4.0/>).

1. Introduction

Submarine oil and gas pipelines serve as the lifelines for offshore oil and gas production systems, providing the most direct and efficient means of transportation [1]. With the increasingly complex exploitation environment and the growing utilization of fiber materials, the application of RTPs based on thermoplastic materials has gained traction in the field of offshore engineering [2–5]. Submarine pipelines, which are partially embedded in the seabed, are subjected to lateral soil resistance during significant lateral movements. This resistance plays a crucial role in the lateral buckling of pipelines under thermal stress [6,7]. Therefore, studying the interaction between RTPs and soil is of paramount importance to ensure on-bottom stability.

In order to achieve an optimal design solution, it is crucial to accurately model the interaction between a pipe and the soil during large-amplitude lateral movements. In

recent years, researchers have focused on studying the pipe–soil interaction for pipes that are shallowly embedded in the seabed with the aid of centrifuge testing. Several models have been proposed specifically for shallowly embedded pipes, considering different soil types such as calcareous sands [8–12] and clays [12–15]. DNV [16] proposed a small-displacement, three-stage soil resistance model. Bruton et al. [17] conducted lateral large pipeline displacement experiments and analyzed the nonlinear characteristics of soil resistance. They categorized the pipe–soil interaction into the breakthrough, unstable, and residual motion stages. Cheuk, White, and Bolton [18] conducted extensive plane strain model tests to measure the response of a partially embedded pipe segment in soft clay subjected to large-amplitude cyclic movements. The tests aimed to simulate the thermal expansion and contraction experienced at a pipeline bend. Colicchio [19] et al. proposed an innovative model for analyzing pipe–soil interaction using the level set technique for a two-phase mixture of sand and water. Dingle, White, and Gaudin [20] researched the lateral breakthrough resistance and residual resistance of soft clay. During the lateral buckling process, significant lateral displacements ranging from approximately 5 to 20 times the pipe diameter may occur. Wang [15,21] developed a dynamic soil resistance model that varies with the buried depth of the pipeline, based on a series of model tests using sand samples from the Bohai Gulf. In fact, the time-varying soil resistances during the pipe–soil interaction are strongly interconnected in both vertical and lateral directions. However, there is currently limited research attention devoted to this issue, and the coupling mechanism requires further exploration.

Wang [22] developed a new formula for predicting residual resistance based on the failure mechanism of pipe–soil interaction during lateral movement. Kong [7] explored the breakout resistances of a pipe in all possible directions to determine the most vulnerable plane where transverse displacement is likely to occur, along with the minimum breakout resistance. Liu [21] conducted large-scale model tests on Bohai sand and proposed bi-linear pipe–soil interaction models normalized by pipe weight and diameter based on these test results. Dong [23] developed a coupled large-deformation finite element (LDFE) framework with a small strain (RITSS) and discussed the effects of the interaction rate and drainage condition on the p – y curve, excess pore pressure generation and dissipation, and failure mechanisms. Liu and Ortega [24] proposed a closed-form linear–elastic solution to analyze pipes that were restrained using both thrust blocks and restrained joints. The solution took into consideration the passive soil resistance, as well as the contribution of friction resistance resulting from the increased normal pressure at the pipe–soil interface. Macaro, Utili, and Martin [25] utilized the three-dimensional distinct-element method to investigate the behavior of a partially embedded pipe segment in sand, and the simulation approach was validated against experimental results. Wu [26] presented a detailed numerical investigation to study the interaction between large-diameter pipes and soil under three typical working conditions. The study aimed to capture the structural mechanical behaviors associated with pipe deformation, soil displacement, and soil pressure. Additionally, a novel method was introduced to investigate soil–pipe interaction in the lateral and vertical directions. This method involved mounting a soil box on a six-degrees-of-freedom (DOF) system. The test results provided evidence of how different loading types affect soil–pipe interaction and demonstrated a strong coupling of the pipe response in the lateral and vertical directions. Wang [27] proposed a formula for predicting the maximum lateral soil resistance based on tests that examined pipe–soil interaction with different initial pipe embedments and weights. Rezadoost and Nassiraei [28] conducted a comprehensive study on the criteria for modeling fiber-reinforced polymer (FRP) using the finite element method. The accuracy of these models was rigorously verified through meticulous comparisons with experimental results.

There has been extensive research on the interaction between steel pipes and soil in this field. However, research on the soil resistance of RTPs moving on the surface of sandy soil remains largely unexplored. Additionally, existing large-displacement lateral testing

devices have various limitations in terms of efficiency. Therefore, there is a need to enhance the research on the interaction between reinforced thermoplastic (RTPs) pipes and soil.

The aim of this study is to address a research gap by designing and manufacturing a test apparatus for investigating the horizontal soil resistance of flexible pipes in response to different initial settlement depths. This apparatus enables the detection of the lateral soil resistance characteristics of pipelines under varying burial conditions. The primary objective is to reveal the correlation between typical resistance and lateral movement at different stages. Moreover, the study aims to resolve the issue of grid distortion caused by soil deformation by employing the CEL method to simulate the interaction between pipes and soil. The effectiveness of the simulation was validated through a comparison with the experimental results.

2. Experimental System and Content

2.1. Experimental Configuration

Typically, pipelines are assumed to be infinitely long, and axial displacements are disregarded, allowing the lateral pipe–soil interaction problem to be simplified as a plane strain problem [29]. Based on this conception, a testing system for lateral pipe–soil interaction was designed to replicate significant lateral movements of the pipe above the seabed, as depicted in Figure 1.

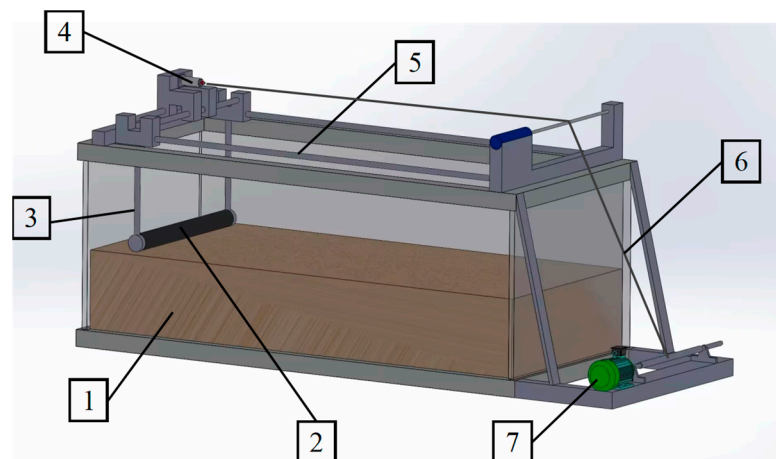


Figure 1. Sketch of the experimental device. 1—soil box; 2—flexible pipe; 3—anti-roll linkage mechanism; 4—tension–compression load sensor; 5—slide (with wiping lubricant); 6—steel wire; and 7—electric motor.

- (1) Experimental system: In a rectangular soil box, two parallel tracks with a length of 1.5 m were built, and a connection structure with a flexible pipeline was designed to connect the pipe to the motive force transmission device and install it on the soil box. The motive force transmission device was connected to the pressure sensor, and the pipeline was driven horizontally in the soil sample to obtain the relationship curve between the pipe displacement and the soil resistance force.

The design of the connecting components between the pipeline and the transmission structure is shown in Figure 2. The connecting mechanism consists of the following components:

- A connecting rod: It provides the structural connection between different parts of the mechanism;
- A connecting outer circle: Its diameter is equal to the outer diameter of the pipeline. It ensures the connection between the mechanism and the outer surface of the pipeline;
- A connecting inner embedded circle: Its diameter is equal to the inner diameter of the pipeline. It ensures the connection between the mechanism and the inner surface of the pipeline;

- An anti-rotation latch: It is embedded in the gap of the pipeline to prevent circumferential movement during horizontal motion of the pipeline.
- (2) Experimental equipment: The main instruments and components used in this experiment included the following: a soil box size whose length \times width \times depth = 1.5 m \times 1.0 m \times 1.0 m, an LTR-1 tension–compression load, sensor, a sliding rail, a pipeline anti-roll and translation device, a motor, etc.
 - (3) Experimental samples: Flexible, non-metallic pipes with a diameter of 76 mm and sandy soil from the seabed.

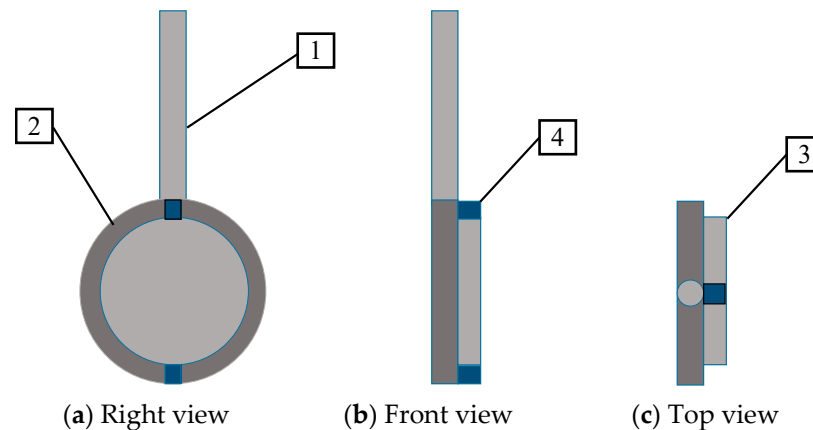


Figure 2. Schematic diagram of the pipe connection. 1—connecting rod, 2—connecting outer circle, 3—connecting inner embedded circle, and 4—anti-rotation latch.

2.2. Experiment Content

This experiment included three parts: (1) carry out soil shear tests to determine the friction angle and shear strength of the soil; (2) carry out pipe–soil interaction experiments to identify the relationship between horizontal pipe displacement and soil resistance; (3) analyze the experimental results based on the scientific research literature and obtain comparative data on the differences in the soil resistance loads of flexible, non-metallic pipes and steel pipes.

2.3. Tests Pipe

The RTPs examined in this study were made up of a polyethylene (PE) matrix with fiberglass reinforcement, as depicted in Figure 3. The reinforcement comprised fiberglass embedded within the polymer matrix, which was spirally wound around the inner PE liner at a specific angle. The layers were fused together through heating, producing a filament-wound fiber-reinforced composite pipe.

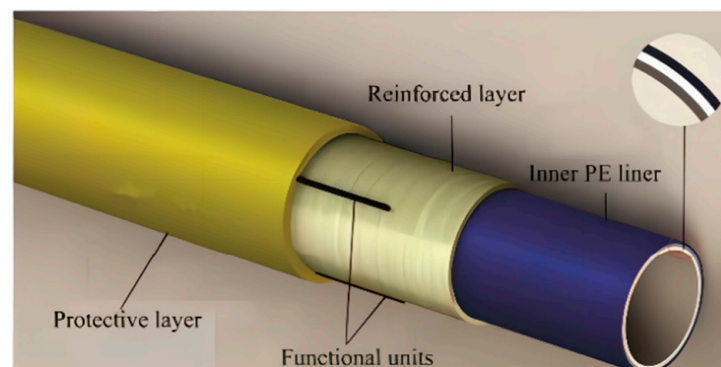


Figure 3. Structural diagram of an RTP.

2.4. Test Soil

The South China Sea is rich in oil and gas storage and transportation, and submarine pipelines have a relatively broad application space. To ensure the safety of submarine pipelines, the target oil and gas sea area of seabed sand was selected as the experimental model, which had a wide particle size distribution. Sandy soil is highly permeable and rapidly drains, resulting in the strength of a dry sample being comparable to that of a saturated sample under drained conditions. Thus, in the interest of simplification, we employed dry sand to construct the test soil bed.

2.5. Experimental Process

To study pipe–soil interactions during large displacements in sand, we conducted two series of tests, a shear strength experiment with soil tests and large-amplitude motion tests.

The main purpose of the shear strength experiment was to identify the mechanical parameters of the experimental soil samples to predict the lateral soil resistance in numerical simulations. The objective of the lateral large displacement experiment was to determine the lateral soil resistance experienced by the pipeline under different initial burial depth conditions.

1. Soil shear strength test:

The purpose of the soil shear strength test was to study the shear strength and internal friction angle of the soil sample. A constant-normal-pressure shear test was carried out at seven normal pressures. After the normal displacement was stable, the shear was started, and the shear rate was controlled at 0.8 mm/min. The target parameters were identified by processing the experimental data, as shown in Figure 4.

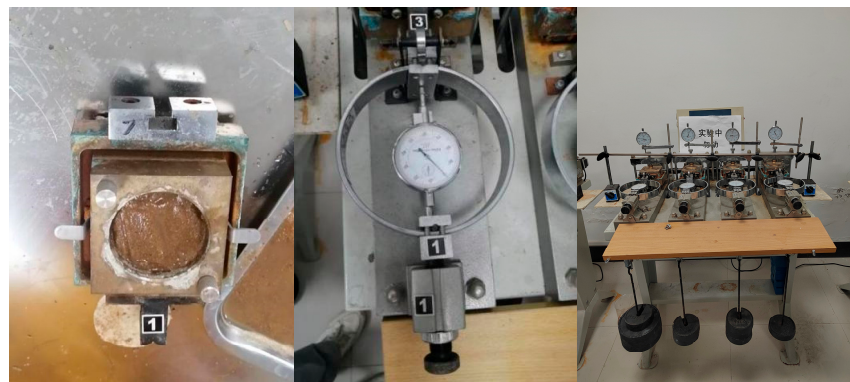


Figure 4. Soil shear test.

2. Pipe–soil interaction experiment:

It has been shown that the impedance of sandy soil to pipelines does not differ significantly between fully wet and fully dry states. Therefore, dry sandy soil was used in this experiment. The experimental system was set up as shown in Figure 5. The surface of the sandy soil was scraped flat, and lubricating oil was applied to the smooth track to reduce the influence of track friction on the experimental results.

The vertical position of the track was adjusted to ensure that the pipeline had initial depths of $0.1D$, $0.2D$, and $0.3D$, where $0.1D$ means 0.1 times the pipe diameter.

The electric motor was started, and the steel wire rope was tightened via the transmission rod to drive the truss structure and the test pipeline to move laterally on the surface of the sandy soil through the auxiliary pulley system. In order to better observe the change in soil resistance, the pipeline always maintained a stable and relatively low speed value during lateral movement. Table 1 shows the experiment parameters.

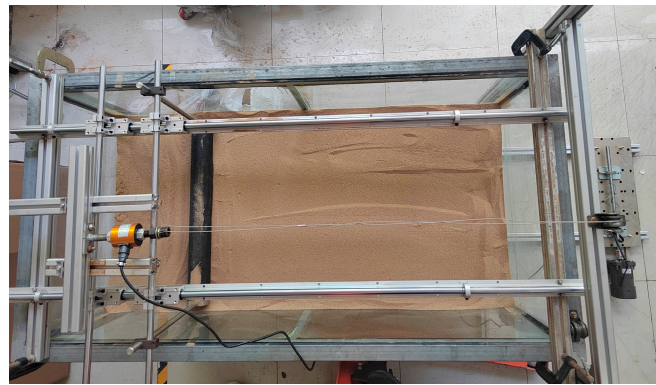


Figure 5. Lateral pipe–soil interaction testing system.

Table 1. Experiment parameters.

Property	Value
Pipe diameter (mm)	76
Internal friction angle (degrees)	To be tested
Cohesive strength (Pa)	To be tested
Soil density (kg·m ⁻³)	1560
Horizontal displacement (mm)	760 (10 times the pipe diameter)
Initial embedment	0.1D, 0.2D, and 0.3D

3. Numerical Method

3.1. CEL Theoretical Approach

The lateral displacement of pipes can cause soil extrusion, which poses challenges for numerical calculations due to material deformation and grid distortion. In order to avoid computational failures caused by conventional methods, this study employed the coupled Eulerian–Lagrangian (CEL) method to address the issue of large deformations in pipe–soil interaction. The CEL method utilizes the Eulerian description of solid mechanics problems. The following are the principles underlying the CEL method.

The Lagrangian formulation was employed to describe the conservation equations for mass, momentum, and energy, which could be expressed as follows:

$$\frac{d\rho}{dt} + \rho \nabla \cdot \mathbf{v} = 0 \tag{1}$$

$$\rho \frac{d\mathbf{v}}{dt} = \nabla \cdot \boldsymbol{\sigma} + \rho \mathbf{b} \tag{2}$$

$$\frac{de_I}{dt} = \boldsymbol{\sigma} : \dot{\boldsymbol{\epsilon}} \tag{3}$$

$$\frac{d\psi(x, t)}{dt} = \frac{\partial \psi(x, t)}{\partial t} + \mathbf{v} \cdot (\nabla \psi(x, t)) \tag{4}$$

In these equations, ρ represents the material density, \mathbf{v} represents the material particle velocity, $\boldsymbol{\sigma}$ represents the Cauchy stress, \mathbf{b} represents body forces, e_I represents the specific internal energy per unit volume, $\dot{\boldsymbol{\epsilon}}$ represents the rate of strain, “:” denotes the double contraction of tensors, ∇ represents the gradient operator, and $\nabla \cdot \mathbf{v}$ represents the divergence of the velocity vector. $\psi(x, t)$ represents the field function.

The Lagrangian control equations were converted into Eulerian-form control equations:

$$\frac{\partial \rho}{\partial t} + \nabla \cdot (\rho \mathbf{v}) = 0 \tag{5}$$

$$\frac{\partial \rho \mathbf{v}}{\partial t} = \nabla \cdot (\rho \mathbf{v} \otimes \mathbf{v}) = \nabla \cdot \boldsymbol{\sigma} + \rho \mathbf{b} \tag{6}$$

$$\frac{\partial e_I}{\partial t} + \nabla \cdot (e_I \mathbf{v}) = \boldsymbol{\sigma} : \dot{\boldsymbol{\epsilon}} \tag{7}$$

$$\frac{\partial \psi}{\partial t} + \nabla \cdot \boldsymbol{\Psi}(\psi, v, x, t) = \mathbf{S} \tag{8}$$

Among them, the term $\boldsymbol{\Psi}$ represents the flux function accounting for convective effects, and \mathbf{S} represents the source term.

In the CEL method, the equation mentioned above was decomposed into two separate equations, and these two equations were solved sequentially in each numerical iteration step.

$$\frac{\partial \psi}{\partial t} = \mathbf{S} \tag{9}$$

$$\frac{\partial \psi}{\partial t} + \nabla \cdot \boldsymbol{\Psi}(\psi, v, x, t) = 0 \tag{10}$$

Using an explicit time integration scheme, the velocity and displacement solutions of the physical problem were computed and updated using the central difference method.

$$\mathbf{v}^{n+1/2} = \mathbf{v}^{n-1/2} + \Delta t \mathbf{M}^{-1} \left\{ \mathbf{F}_{external}^n - \int \mathbf{B}^T \bar{\boldsymbol{\sigma}} d\Omega \right\} \tag{11}$$

$$\mathbf{x}^{n+1} = \mathbf{x}^n + \Delta t \mathbf{v}^{n+1/2} \tag{12}$$

In these equations, \mathbf{M} represents the mass diagonal matrix, $\mathbf{F}_{external}^n$ represents the external force vector, \mathbf{B} represents the strain matrix, $\bar{\boldsymbol{\sigma}}$ represents the average stress within the element, n represents the n th time increment step, Ω represents the computational domain, and Δt represents the duration of the n th time increment step.

3.2. Modeling Criteria

a. Constitutive Model

The Mohr–Coulomb model was employed to the constitutive relationship for the soil in this study. The soil domain and air domain were discretized using Eulerian elements, while the pipe model was represented using Lagrangian elements. The structure mesh and fluid mesh were coupled using the CEL contact algorithm to enable the numerical simulation of large lateral displacements in the pipe–soil system.

b. Pipe–Soil Interaction

This approach was based on the time-domain dynamic analysis method to investigate the pipe–soil interaction. In order to prevent the settlement of the soil under its own weight and ensure the relative stability of the soil properties, the loading was applied through internal forces between the soil layers. This loading method allowed the formation of an initial stress field in the soil that satisfied the given conditions and achieved stress equilibrium.

c. Modeling Dimension Verification

Considering the influence of the grid scale on computational results, it is necessary to investigate the sensitivity of the grid size in the soil–pipe interaction region. Taking the self-weight settlement of the pipeline as a case study, this research analyzed the temporal variation curve of the soil–pipe interaction force and compared the effects of different grid sizes on the unit length of soil reaction. Three scenarios were selected for calculation: a large grid (8 mm), a medium grid (5 mm), and a small grid (3 mm). The results indicate that the soil–pipe interaction forces converged and exhibited relatively consistent mean values

in all three scenarios, as per Figure 6. However, the large grid (8 mm) showed significant fluctuations during the stable phase, while the medium and small grids exhibited smoother variations. The computational cost of the small grid was approximately 4.5 times higher than that of the medium grid. Therefore, to obtain accurate results with a relatively small computational workload, it is recommended to set the soil grid size to 5 mm and gradually transition towards the surrounding boundaries.

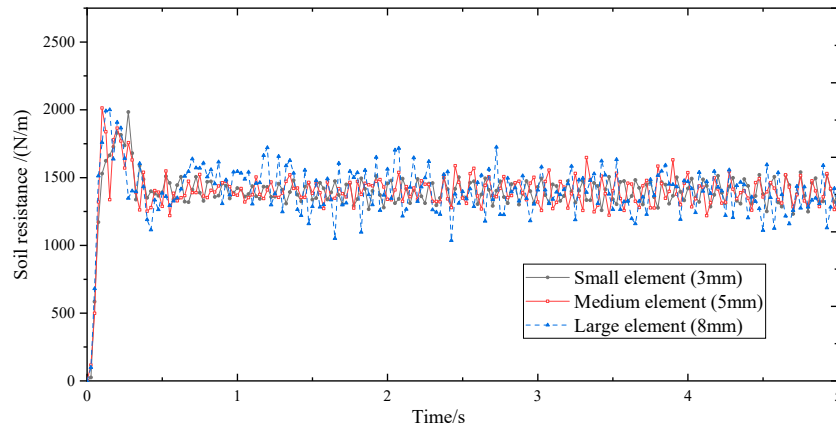


Figure 6. Analysis of grid sensitivity in the CEL method.

4. Results and Discussion

4.1. The Results of the Soil Shear Strength Test

The force readings of the measuring ring under different normal pressures are shown in Table 2, and the shear strength and vertical pressure relationship curve is shown in Figure 7, which identified the friction angle and cohesive force of the soil sample.

Table 2. Shear strength experimental data.

No.	Normal Pressure (kPa)	Load Coefficient (kPa·mm ⁻¹)	Load Measurement (mm)	Shear Pressure (kPa)
1	100	1.572	34.72	54.58
2	150	1.558	70.69	110.13
3	200	1.572	83.18	130.76
4	250	1.585	98.69	156.42
5	300	1.585	122.29	193.83
6	350	1.558	141.50	220.46
7	400	1.558	166.90	260.03

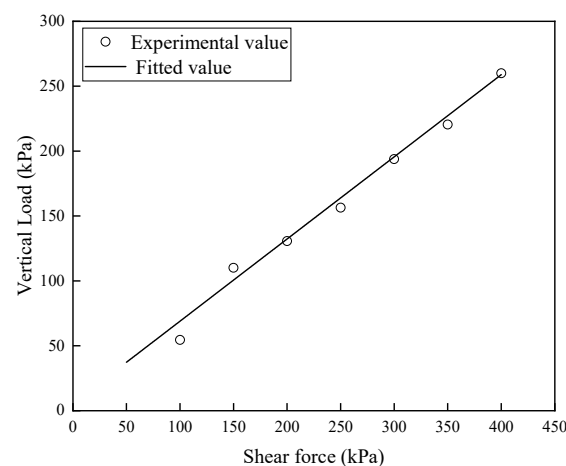


Figure 7. Shear force–vertical load relationship curve.

The experimental data were fitted using the linear fitting method. The intercept of the curve at the y-axis for the lateral displacement of the pipeline at different depths was found to be 0.158, with a slope of $k = 0.6429$. The cohesive force was found to be 0.158 kPa, and the internal friction angle was found to be 32.75° .

4.2. Pipe-Soil Interaction Experiment Results

(1) Experimental phenomena:

Based on the analysis of experimental observations shown in Figure 8, the following conclusions can be drawn. At the initial settlement position, the pipeline maintained its position stability under the influence of soil resistance (Figure 8a). Under lateral displacement, the soil resistance increased with the rise of the soil bulging height. With small displacements (Figure 8b), the soil resistance exhibited a typical softening response. The soil bulged around the pipeline, leading to soil damage, uplift, and accumulation on the movement side, resulting in an increase in the soil height.

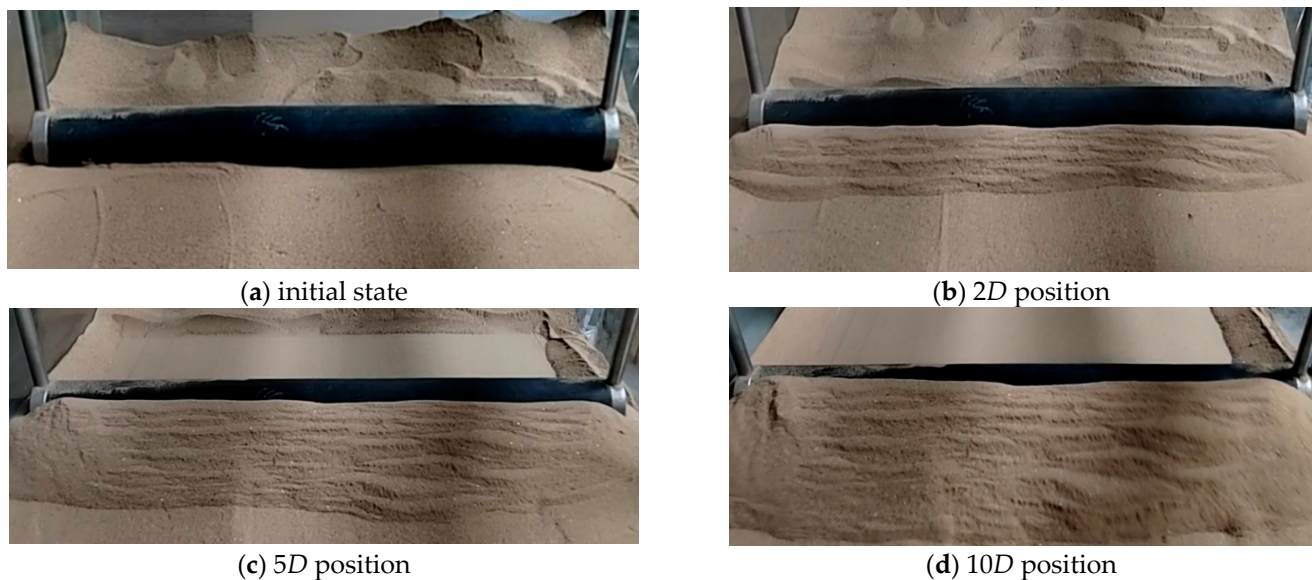


Figure 8. Soil failure at lateral displacements in the 3D initial embedment.

As the lateral displacement increased (Figure 8c), the accumulation of the soil expanded the failure range, enhancing the resistance to the lateral displacement of the simulated pipeline. When the lateral displacement further increased (Figure 8d), the accumulated soil on top of the pipeline could not be sustained, leading to detachment. The degree of detachment was dependent on the cohesive strength of the soil layer.

(2) Experimental data

Figure 9 shows the curve of lateral soil resistance measured during the experiment for a 76-mm-diameter pipeline at different initial depths and horizontal displacements.

From the analysis of the collected experimental data, it could be observed that, at a fixed burial depth, during the initial stage where the lateral displacement was within the range of $0.5D$, the lateral soil resistance rapidly increased and gradually increased with the increase in the horizontal displacement of the pipeline. This is because, during the initial stage, the pipeline remained within the range of the in-place stability capacity. However, when the displacement exceeded $0.5D$, the pipeline transitioned into a phase of overall large deformation. As the lateral displacement of the pipeline increased, the front soil sample gradually bulged, causing the soil resistance to increase gradually with the displacement as the pipeline moves laterally. This increase in the soil resistance was closely related to the gradual rise in the height of the front soil.

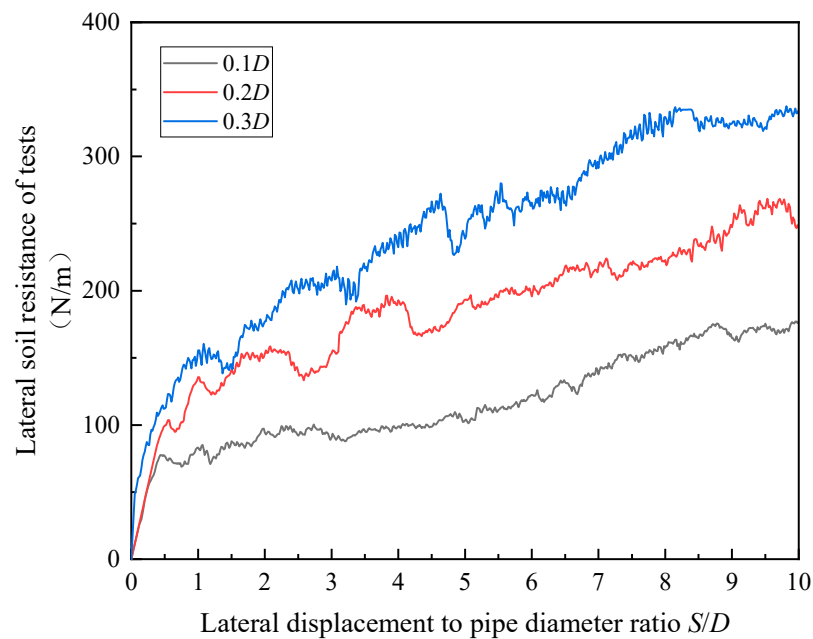


Figure 9. Lateral soil resistance curve of the tests.

Based on the analysis of the experimental results from pipelines with different initial burial depths, it could be observed that, as the initial settlement depth of the pipeline increased, the rate of increase in the soil resistance during the pipeline initiation stage was higher, and the final lateral soil resistance at 10D displacement was also greater. The soil resistance values obtained from the experiments are shown in Table 3, and the peak soil resistance between adjacent test conditions decreased.

Table 3. Soil resistance measured via tests.

No.	Initial Embedment	Soil Resistance/N	Difference/N
1	0.1D	160.38	—
2	0.2D	252.69	92.30
3	0.3D	315.77	63.07

In order to obtain a more accurate numerical simulation method for the interaction between pipes and the soil, this study employed the CEL method to numerically simulate the resistance of pipe–soil interaction. The simulation was conducted using an initial burial depth of 0.5D as an example. The deformation of the soil is presented in Figure 10. The results indicate that, at a lateral displacement of 0.5D (Figure 10a), there was a noticeable uplift of the soil, with a significant increase in height compared to its initial horizontal position. When the displacement reached 2D (Figure 10b), the height of the soil was approximately equal to the pipe diameter. As the displacement gradually increased to 4D (Figure 10c), the soil continued to accumulate above the pipe, and the horizontal width of the uplifted soil also increased, consistent with the experimental observations. When the lateral displacement reached 7D (Figure 10d), the accumulated soil above the pipe underwent failure, resulting in soil detachment towards the opposite movement side. Subsequently, the soil’s interaction force reached a stable state.

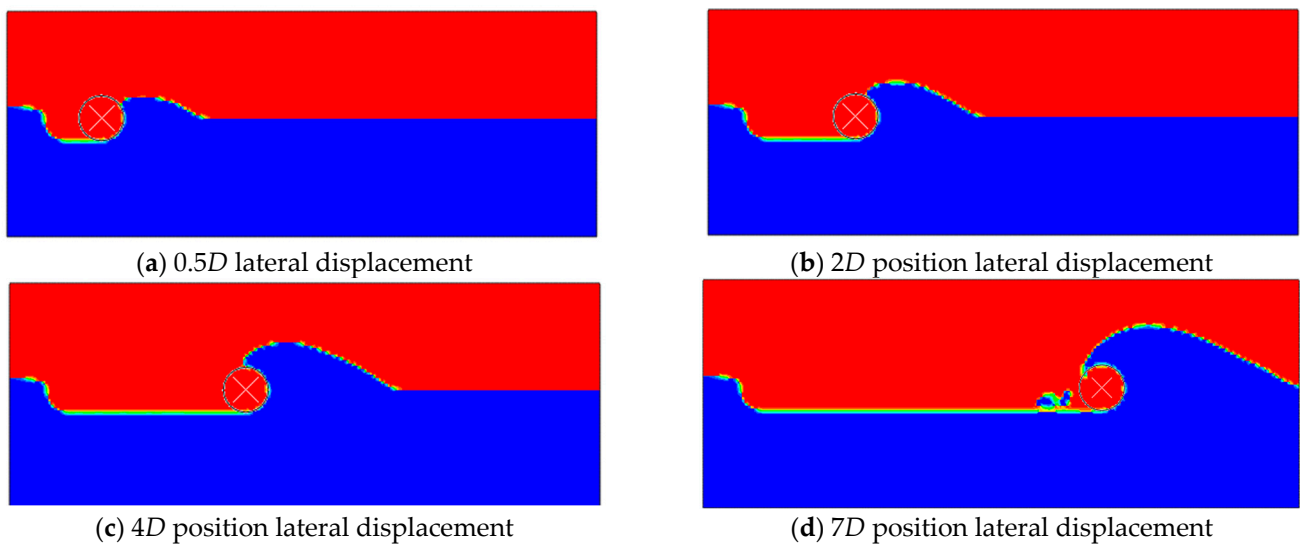


Figure 10. Soil failure with lateral displacement in $0.5D$ via a numerical simulation.

Figure 11 presents schematic diagrams of the lateral and axial pipe–soil interaction at a lateral displacement of $7D$ in the model experiments. From the figure, it can be observed that the height of the soil bulging in the direction of the pipeline displacement gradually increased with the increase in lateral displacement. The height of the soil bulging approached approximately 1.5 times the diameter of the pipeline. As shown in Figure 11a, the distribution of the soil bulging height along the length direction was not uniformly consistent, which was attributed to the initial non-uniformity of the soil layer height in the experimental setup. During the model experiments, soil detachment began to occur at the $7D$ position (Figure 11b), which was consistent with the numerical simulation results and the observed phenomenon.



(a) $7D$ position lateral displacement (test)



(b) $7D$ position lateral displacement (test)

Figure 11. Height of soil bulging.

Figure 12 illustrates the soil resistance curves at different burial depths, based on the CEL method. The results show that the ultimate soil resistance increased in a sequential manner with the increase in burial depth. The numerical simulation results demonstrate that, within the lateral displacement range of the initial $0.5D$, the soil resistance increased sharply. In the initial stage, the pipeline was positioned within the trench, and under external forces, it was required to overcome the lateral soil resistance, resulting in lateral displacement. Therefore, the soil resistance rapidly increased from zero, reaching its peak growth rate within approximately $0.2D$. As the lateral displacement continued to increase, the soil resistance force continued to rise, but at a diminishing growth rate.

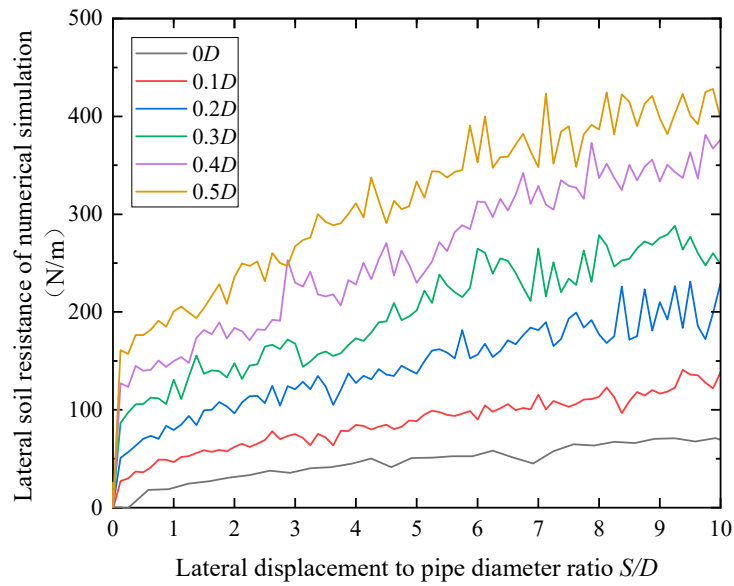


Figure 12. Lateral soil resistance curve of the simulation.

For the conditions of $0D$, $0.1D$, $0.2D$, $0.3D$, and $0.4D$, the soil resistance continued to increase with the displacement, and it exhibits an upward trend even at the $10D$ position. Under the $0.5D$ condition, a distinct phase of cyclically stable soil resistance was observed. This is because only under the $0.5D$ condition did the soil reach the critical state of soil detachment failure. A comparison between the calculated soil resistance results based on the CEL method and the experimental data is shown in Figure 13. It is evident that the experimental soil resistance values are higher than the numerical simulation results. Table 4 presents the corresponding numerical calculation results of the simulation and experimental data, indicating a discrepancy that decreased with increasing burial depth, reaching approximately 10%. This difference was attributed to the influence of frictional resistance in the sliding device mechanism, which decreased in proportion as the burial depth increased. The computational results demonstrate that the proposed CEL method in this study achieves good accuracy in predicting pipe–soil interaction forces and effectively addresses the issue of distorted finite element meshes, thereby accurately representing the deformation and flow characteristics of the soil.

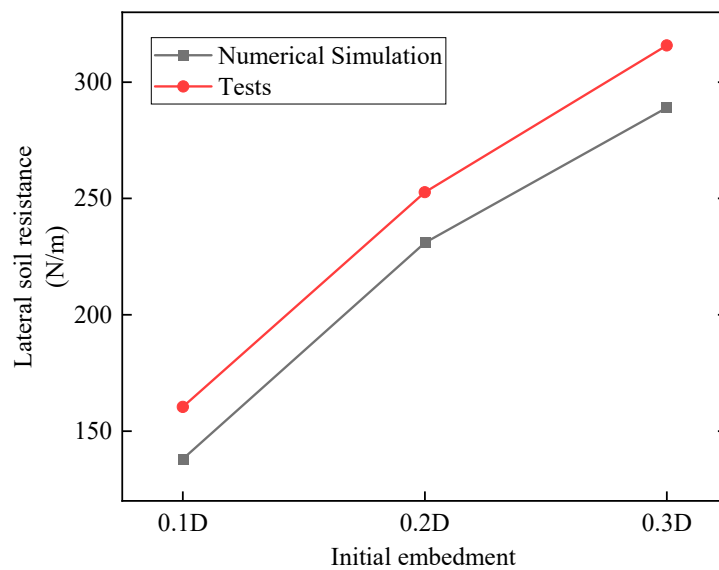


Figure 13. Comparison between the simulation of and experiment on soil resistance.

Table 4. Difference between the simulation of and experiment on soil resistance.

No.	Initial Embedment	Numerical Simulation/N	Tests/N	Difference/N
1	0.1D	138	160.38	13.9%
2	0.2D	231	252.69	8.6%
3	0.3D	289	315.77	8.5%

5. Conclusions

This study designed and conducted enhanced experimental tests on the mechanical interaction between reinforced flexible pipes and sandy soil. The magnitudes of the soil resistance acting on the pipes were measured for both exposure and different burial depths. A simulation method for lateral soil resistance based on the CEL method was developed. The conclusions are as follows:

- (1) Within the lateral displacement range of $0.5D$, the lateral soil resistance increases rapidly. As the lateral displacement of the pipe increases, the soil climbs along the circumferential direction of the pipe, increasing the load-bearing capacity of the pipe and the accumulated soil resistance. The accumulation of soil leads to a larger range of soil failure.
- (2) With an increase in the burial depth, the ultimate soil resistance exhibits an increasing sequence, and the final uplifted height of the soil reaches a critical state. A larger initial burial depth allows for a quicker attainment of the critical soil resistance state. The differences in the final soil resistance among different burial depths decrease gradually, and this conclusion was validated through data calculations.
- (3) The CEL method successfully addresses the issue of grid distortion caused by soil deformation and effectively simulates the pipe–soil interaction forces under large lateral displacements. The results of the simulation align well with the experimental findings, demonstrating the effectiveness of this method from both qualitative and quantitative perspectives.

Author Contributions: Conceptualization, C.W.; methodology, C.W.; software, L.L.; validation, Y.Z. and L.L.; formal analysis, C.W.; investigation, M.L.; data curation, C.W.; writing—original draft preparation, Y.Z. and L.L.; writing—review and editing, C.W.; supervision, M.L.; project administration, C.W.; funding acquisition, M.L. All authors have read and agreed to the published version of the manuscript.

Funding: This research was funded by the following: the National Natural Science Foundation of China, grant number U2006226; the National Key Research and Development Program of China, grant number 2016YFC0303800; Fundamental Research Funds for the Central Universities, grant number 20CX02320A; and the Opening Fund of National Engineering Laboratory of Offshore Geophysical and Exploration Equipment.

Institutional Review Board Statement: Not applicable.

Informed Consent Statement: Not applicable.

Data Availability Statement: Data are contained within the article.

Conflicts of Interest: The authors declare no conflict of interest.

References

1. Bai, Y.; Liu, T. Mechanical behavior of metallic strip flexible pipe subjected to tension. *Compos. Struct.* **2017**, *170*, 1–10. [[CrossRef](#)]
2. Bai, Y.; Tang, J. Collapse of reinforced thermoplastic pipe (RTP) under combined external pressure and bending moment. *Ocean Eng.* **2015**, *94*, 10–18. [[CrossRef](#)]
3. Wang, Y.Y.; Lou, M.; Tong, B.; Wang, S. Mechanical properties study of reinforced thermoplastic pipes under a tensile load. *China Ocean Eng.* **2020**, *34*, 806–816. [[CrossRef](#)]
4. Bai, Y.; Wang, Y.; Cheng, P. Analysis of Reinforced Thermoplastic Pipe (RTP) under Axial Loads. *Iliffe* **2012**, 708–724. [[CrossRef](#)]

5. Lou, M.; Wang, Y.; Tong, B. Effect of temperature on tensile properties of reinforced thermoplastic pipes. *Compos. Struct.* **2020**, *241*, 112119. [[CrossRef](#)]
6. Li, C.F.; Liu, R. Experimental and theoretical studies on lateral buckling of submarine pipelines. *Mar. Struct.* **2021**, *78*, 102983. [[CrossRef](#)]
7. Kong, D.Q.; Feng, L.Y.; Zhu, B. Assessment model of pipe soil interaction during large-amplitude lateral displacements for deep-water pipelines. *Comput. Geotech.* **2020**, *117*, 103220. [[CrossRef](#)]
8. Tian, Y.H.; Cassidy, M.J.; Gaudin, C. Advancing pipe-soil interaction models in calcareous sand. *Appl. Ocean Res.* **2010**, *32*, 284–297. [[CrossRef](#)]
9. Calvetti, F.; di Prisco, C.; Nova, R. Experimental and numerical analysis of soil-pipe interaction. *J. Geotech. Geoenviron. Eng.* **2004**, *130*, 1292–1299. [[CrossRef](#)]
10. Zhang, J.G.; Stewart, D.P.; Randolph, M.F. Modeling of shallowly embedded offshore pipelines in calcareous sand. *J. Geotech. Geoenviron. Eng.* **2002**, *128*, 363–371. [[CrossRef](#)]
11. Tian, Y.H.; Cassidy, M.J. Modeling of Pipe-Soil Interaction and Its Application in Numerical Simulation. *Int. J. Geomech.* **2008**, *8*, 213–229. [[CrossRef](#)]
12. White, D.J.; Dingle, H.R.C. The mechanism of steady friction between seabed pipelines and clay soils. *Geotechnique* **2011**, *61*, 1035–1041. [[CrossRef](#)]
13. Hodder, M.S.; Cassidy, M.J. A plasticity model for predicting the vertical and lateral behaviour of pipelines in clay soils. *Geotechnique* **2010**, *60*, 247–263. [[CrossRef](#)]
14. Bienen, B.; Cassidy, M.J. Advances in the three-dimensional fluid-structure-soil interaction analysis of offshore jack-up structures. *Mar. Struct.* **2006**, *19*, 110–140. [[CrossRef](#)]
15. Wang, L.; Liu, R. The effect of a berm on the lateral resistance of a shallow pipeline buried in sand. *Ocean Eng.* **2016**, *121*, 13–23. [[CrossRef](#)]
16. Det Norske Veritas. *On-Bottom Stability Design of Submarine Pipelines*; Det Norske Veritas Group: Oslo, Norway, 2021.
17. Bruton, D.; White, D. Pipe/Soil Interaction Behavior During Lateral Buckling. *Sex. Abuse J. Res. Treat.* **2006**, *21*, 57–75. [[CrossRef](#)]
18. Cheuk, C.Y.; White, D.J.; Bolton, M.D. Large-scale modelling of soil-pipe interaction during large amplitude cyclic movements of partially embedded pipelines. *Can. Geotech. J.* **2007**, *44*, 977–996. [[CrossRef](#)]
19. Colicchio, G.; Colagrossi, A. Pipe-soil interaction: An evaluation of a numerical model. In Proceedings of the 26th International Conference on Offshore Mechanics and Arctic Engineering (OMAE 2007), San Diego, CA, USA, 10 June 2007.
20. Dingle, H.R.C.; White, D.J.; Gaudin, C. Mechanisms of pipe embedment and lateral breakout on soft clay. *Can. Geotech. J.* **2008**, *45*, 636–652. [[CrossRef](#)]
21. Liu, R.; Liu, W. A soil resistance model for subsea pipeline global lateral buckling analysis. *Rock Soil Mech.* **2015**, *36*, 2433–2441.
22. Wang, Z.K.; Tang, Y.G. Model Test for Lateral Soil Resistance of Partially Embedded Subsea Pipelines on Sand during Large-Amplitude Lateral Movement. *J. Coast. Res.* **2017**, *33*, 607–618. [[CrossRef](#)]
23. Dong, X.Y.; Zhang, W.C. Large deformation coupled analysis of embedded pipeline-Soil lateral interaction. *Mar. Struct.* **2021**, *78*, 102971. [[CrossRef](#)]
24. Liu, M.; Ortega, R. Thrust Restraint of Buried Continuous Pressure Pipe Considering Pipe-Soil Interaction. *J. Pipel. Syst. Eng. Pract.* **2021**, *12*, 04021039. [[CrossRef](#)]
25. Macaro, G.; Utili, S.; Martin, C.M. DEM simulations of transverse pipe-soil interaction on sand. *Geotechnique* **2021**, *71*, 189–204. [[CrossRef](#)]
26. Wu, H.G.; Yu, J.H. Pipe-Soil Interaction and Sensitivity Study of Large-Diameter Buried Steel Pipes. *KSCE J. Civ. Eng.* **2021**, *25*, 793–804. [[CrossRef](#)]
27. Wang, L.; Wang, Y.F. Physical model tests of lateral pipe-soil interaction including the pipe trajectory in sand. *Eur. J. Environ. Civ. Eng.* **2022**, *26*, 1962–1976. [[CrossRef](#)]
28. Rezadoost, P.; Nassiraei, H. Identification of the most suitable probability distributions for ultimate strength of FRP-strengthened X-shaped tubular joints under axial loads. *Ocean Eng.* **2023**, *290*, 116292. [[CrossRef](#)]
29. Merifield, R.; White, D.J.; Randolph, M.F. The ultimate undrained resistance of partially embedded pipelines. *Geotechnique* **2008**, *58*, 461–470. [[CrossRef](#)]

Disclaimer/Publisher’s Note: The statements, opinions and data contained in all publications are solely those of the individual author(s) and contributor(s) and not of MDPI and/or the editor(s). MDPI and/or the editor(s) disclaim responsibility for any injury to people or property resulting from any ideas, methods, instructions or products referred to in the content.